



LAWRENCE
LIVERMORE
NATIONAL
LABORATORY

Effect of non-axisymmetric magnetic perturbations on divertor heat and particle flux profiles

J. W. Ahn, J. M. Canik, R. Maingi, T. K. Gray, J. D. Lore, A. G. McLean, J. Park, A. L. Roquemore, V. A. Soukhanovskii

September 29, 2010

23rd IAEA Fusion Energy Conference
Daejeon, South Korea
October 11, 2010 through October 16, 2010

Disclaimer

This document was prepared as an account of work sponsored by an agency of the United States government. Neither the United States government nor Lawrence Livermore National Security, LLC, nor any of their employees makes any warranty, expressed or implied, or assumes any legal liability or responsibility for the accuracy, completeness, or usefulness of any information, apparatus, product, or process disclosed, or represents that its use would not infringe privately owned rights. Reference herein to any specific commercial product, process, or service by trade name, trademark, manufacturer, or otherwise does not necessarily constitute or imply its endorsement, recommendation, or favoring by the United States government or Lawrence Livermore National Security, LLC. The views and opinions of authors expressed herein do not necessarily state or reflect those of the United States government or Lawrence Livermore National Security, LLC, and shall not be used for advertising or product endorsement purposes.

Effect of non-axisymmetric magnetic perturbations on divertor heat and particle flux profiles

J.-W. Ahn¹, J.M. Canik¹, R. Maingi¹, T.K. Gray¹, J.D. Lore¹, A.G. McLean¹, J.-K. Park², A.L. Roquemore², and V.A. Soukhanovskii³

¹*Oak Ridge National Laboratory, Oak Ridge, TN 37831, USA*

²*Princeton Plasma Physics Laboratory, Princeton, NJ 08543, USA*

³*Lawrence Livermore National Laboratory, Livermore, CA 94551, USA*

Abstract

Small, non-axisymmetric magnetic perturbations generated by external coils have been found to break the axisymmetry of heat and particle flux deposition pattern in the divertor area in the National Spherical Torus Experiment. The applied 3-D field causes strike point splitting that is represented as local peaks and valleys in the divertor profiles. The phase rotation of the applied $n=1$ fields provides a direct evidence of non-axisymmetric heat and particle deposition. The vacuum field line tracing showed good agreement with the measured heat and particle flux profiles. The plasma response was calculated by the IPEC code and was included in the field line tracing in an $n=3$ perturbation case, demonstrating that it does not significantly affect the location and spacing of the split strike points at the divertor surface. The plasma parameter scan showed that higher toroidal mode number of the applied perturbation and q_{95} produce more striations in the divertor profiles. A modest level of divertor profile modification is found to occur even without the application of 3-D fields in certain high triangularity ($\delta=0.65-0.8$) discharges; application of 3-D fields amplifies the same local peaks and valleys. The connection length profile from field line tracing shows that the radial location of local peaks agrees well with the measurement, also identifying intrinsic error field as a possible source of intrinsic strike point splitting. Finally, the radial location of local peaks in the profiles during the triggered ELMs by the applied 3-D field stays similar before and after the application. This shows that the heat flux from the triggered ELMs appears to follow the mode number of the applied perturbation.

1. Introduction

It was recently found that small, non-axisymmetric magnetic field perturbations produced by internal or external coils can break the toroidal symmetry of divertor heat and particle deposition in tokamaks, generating striated heat and particle footprints at the divertor surface, e.g. in DIII-D [1,2,3] and National Spherical Torus Experiment (NSTX) [4]. This is a direct consequence of the „strike point (SP) splitting“ caused by the 3-D magnetic field

perturbations to the plasma edge [1]. As many tokamak plasma facing components (PFCs) are designed and built assuming toroidal symmetry to protect areas where high heat and particle fluxes are expected from the 2-D equilibrium, these non-axisymmetric, i.e., 3-D, divertor profiles could result in additional engineering constraints. These applied 3-D magnetic perturbations are also found to suppress [5] or mitigate [6] ELMs in conventional tokamaks, while they trigger ELMs in spherical tokamaks [7,8]. In NSTX, the 3-D field perturbation was applied to ELM-free H-mode plasmas achieved with lithium (Li) wall coatings of the plasma facing components [9], in order to trigger controlled ELMs with the goal of flushing impurities and reducing radiated power from the core plasma [10]. It is therefore important to investigate the effect of 3-D field on heat and particle flux profiles during and between ELMs and their relation to a wide range of plasma parameters.

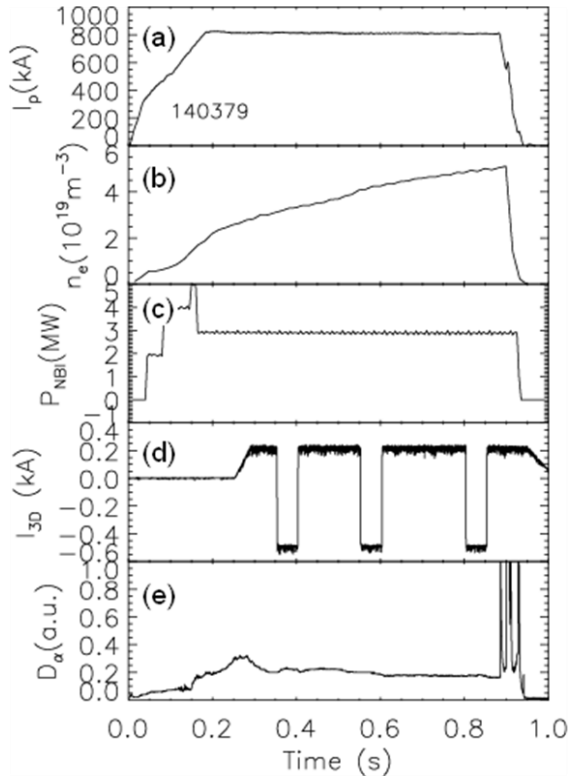


Figure 1 Time evolution of various discharge parameters for a 3-D field applied shot: (a) plasma current, (b) line averaged density, (c) injected NBI power, (d) current in the external 3-D coil, (e) D_α signal for lower divertor. Note that the 3-D field coil was switched on at 350, 550, and 800ms to -0.5kA and lasted for 50ms to give $n=3$ perturbation field.

positive angle is measured counter-clockwise from the reference point. The IR camera is installed at the toroidal angle $\varphi=135^\circ$. The camera takes IR images of the lower divertor

2. Experimental set-up and measurement technique

The 3-D perturbation fields were generated with a set of six midplane coils, external but close-fitting to the vacuum vessel, that are typically used for error field correction and resistive wall mode feedback control [11,12]. The coils were configured to apply an $n=3$ field in the ELM-destabilization experiments, with a generated magnetic perturbation at the separatrix, $\delta B/B=0.6-0.7\%$ for the peak δB at the coil centre and in the order of 0.1% for the integrated δB over the coil surface. The poloidal spectrum of the applied magnetic perturbation is broad at the plasma edge [8], reaching high enough mode numbers to be resonant with high edge safety factor values ($q_{95}\sim 11$).

The heat flux measurement is made with an SBF-161 infrared (IR) camera [13]. The reference point of the toroidal angle is located at the centre of the midplane coil #1,

plates in 2-D with a temporal resolution of 1.6 to 6.3 kHz, depending on the frame size. The camera measures surface IR emission, which passes through a newly installed dual band IR adaptor [14] to take a ratio between long wavelength (7-10 μ m) and medium wavelength (4-6 μ m) IR intensities. This ratio is converted to surface temperature from bench and in-situ calibrations. A 2-D heat conduction code called THEODOR [15] is used to calculate the divertor heat flux profile from the measured surface temperature. The two dimensions are radial and tile depth directions for tiles with finite thickness as well as taking account of temperature dependent material parameters. However, the effect of Li coatings on the surface emissivity has not been properly assessed for the data presented in this paper, because the condition of Li coated surfaces varies with plasma conditions, and the surface temperature is uncalibrated. Therefore, the heat flux data computed from the surface temperature is not

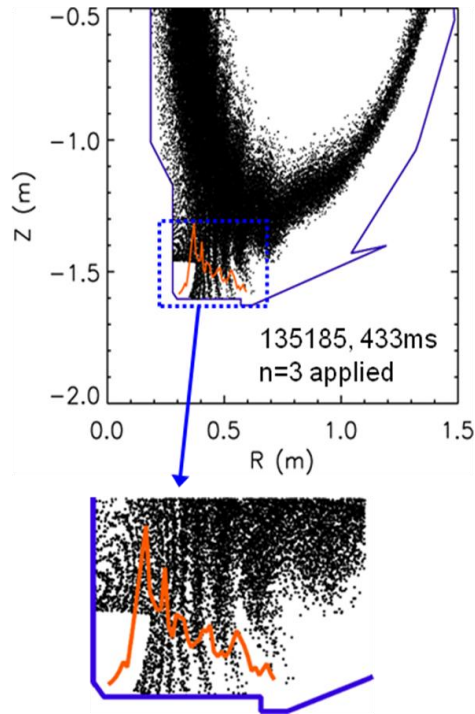


Figure 2 Puncture plot of magnetic field lines for an $n=3$ perturbation application, calculated by a vacuum field line tracing code for the toroidal location of the IR camera at $\varphi=135^\circ$, with the measured heat flux profile overlaid (orange).

absolutely calibrated either. We thus rely on relative comparison of heat flux profiles as 3-D fields are applied. The several kHz framing rate enables heat flux measurement of transient events, such as ELMs and disruptions. The fast framing rate also facilitates measurement of the formation of striations in the divertor heat flux footprints, which can start to appear within 3-4ms after initiation of the 3-D field coil.

The D_α emission at the lower divertor target is recorded by a 1-D CCD camera installed at $\varphi=255^\circ$. It is operated at 2kHz rate and with ~ 0.5 mm spatial resolution and is a part of a system of CCD arrays [16]. The derivation of particle flux from the D_α measurement has been carried out in NSTX [17], with an assumed S/XB coefficient of 20 to convert photon flux to particle flux. Also the divertor recycling coefficient with Li has been estimated from the SOLPS modelling [18] to be $R \sim 0.92$, compared to $R \sim 0.98$ without Li. The outer midplane electron temperature and density at the separatrix for these plasmas are normally $T_{e,sep} = 40-60$ eV, $n_{e,sep} \sim 1 \times 10^{19} \text{m}^{-3}$.

3. Data analysis and interpretation

Figure 1 shows the temporal evolution of an ELM-free H-mode discharge, enabled with Li wall coatings, and with an $n=3$ perturbation field applied. The L-H transition is

indicated by the drop of divertor D_α emission at ~ 130 ms, and the H-mode was sustained until ~ 880 ms. The 3-D field perturbation was applied at 350, 550, and 800ms with constant amplitude of -0.7 kA, on top of the static $n=3$ error field correction current of 0.2kA. The amplitude of the coil current is below the ELM triggering threshold. The line-average electron density continued to rise in the H-mode phase and did not appear to be affected by the 3-D field application.

3.1 Breaking of axisymmetry of divertor heat and particle deposition by 3-D magnetic perturbation

The strike point splitting caused by the applied $n=3$ magnetic perturbation is reflected as local peaks and valleys in the divertor heat flux profile and is measured by the IR camera. Figure 2 shows a comparison of the heat flux profile with a puncture plot from a field line tracing calculation, for the toroidal angle of the IR camera. It is seen that the main characteristics of the heat flux profiles do follow the vacuum field line tracing results, both in the number of the observed striations, and in the relative spacing of the peaks. The inclusion

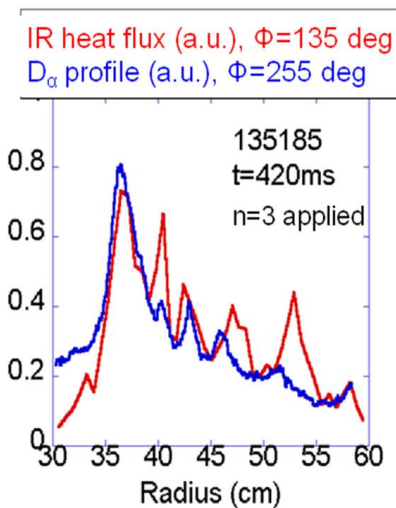


Figure 4 Heat and particle flux profiles measured by IR and D_α cameras at different toroidal angles, $\phi=135^\circ$ and 255° , respectively.

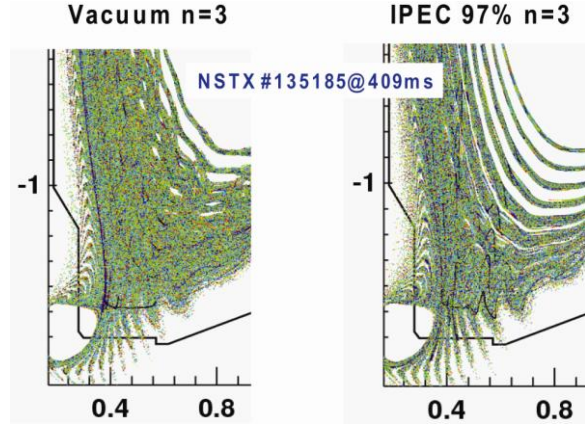


Figure 3 Poloidal Poincare plot from a vacuum field line tracing calculation (left) and from the one with the plasma response included in the field line tracing, up to 97% of normalized flux (eg, $\Psi_N=0.97$) inside the separatrix, calculated by IPEC (right).

of the plasma response inside the unperturbed separatrix by the Ideal Perturbed Equilibrium Code (IPEC) calculation [19] did not affect the structure of split strike points significantly, i.e., the number and radial location of the generated lobes are unchanged relative to the vacuum field calculation (see figure 3). Here, the B-field generated by the plasma current up to a certain fraction of normalized flux (eg, $\Psi_N=0.97$) inside the separatrix is calculated by IPEC and is superposed to the vacuum field to begin field line tracing. This result implies that the open field lines are necessary to explain the divertor striations observed in the experiment, as was pointed out by an EMC3-Eirene modelling [2] that a weak level of cross field transport is needed for the striations to occur, supporting the idea of open field lines.

Toroidal displacement of the IR and D_α cameras by 120° is expected to produce $n=3$ periodicity in the divertor fluxes if the generated lobe structure is consistent with the imposed

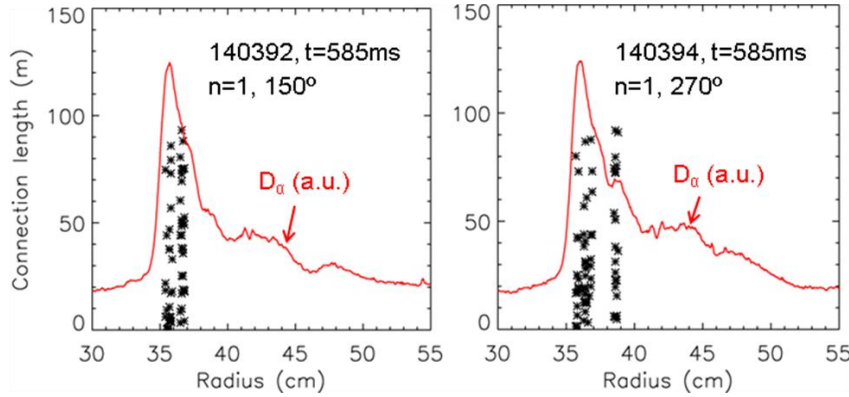


Figure 5 Magnetic footprints on the divertor target, calculated by vacuum field line tracing (black asterisks) and measured D_α profile at the toroidal location of $\varphi=255^\circ$, for two different phase angles of 150° (left) and 270° (right).

between field line tracing and D_α profile for two phase angle of applied $n=1$ field, 150° and 270° . The field line tracing shows different connection length profiles for the two phase angles, caused by non-axisymmetric $n=1$ fields with different toroidal phases. Indeed, an additional local peak at the radial location of ~ 38.5 cm for the phase angle of 270° is expected and confirmed by the measurement in figure 5.

The divertor profiles show a moderate level of strike point splitting even before the application of external magnetic perturbation in some high δ discharges. The profiles show nearly monotonic decay, i.e., no strike point splitting, during the early stage of the discharge typically until $t \sim 200$ ms and then begin to develop local peaks and valleys in the scrape-off layer region. The degree of splitting varies in time, and both the heat flux and D_α profiles

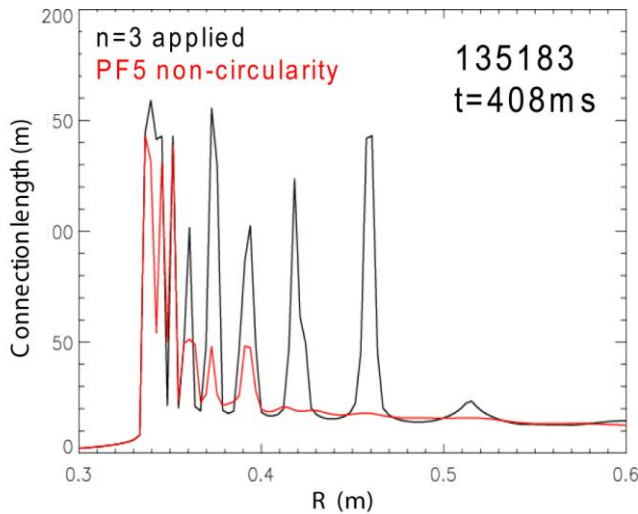


Figure 6 Comparison of computed connection length profiles between $n=3$ field applied (black) and the PF5 intrinsic error field (red) cases.

$n=3$ field structure.

Indeed, the temporal and spatial evolution of striations is very similar for both heat flux and D_α profiles (see figure 4).

Application of $n=1$ fields provides even more direct evidence of the imposed toroidal asymmetry. Figure 5 shows comparison

between field line tracing and D_α profile for two phase angle of applied $n=1$ field, 150° and 270° . The field line tracing shows different connection length profiles for the two phase angles, caused by non-axisymmetric $n=1$ fields with different toroidal phases. Indeed, an additional local peak at the radial location of ~ 38.5 cm for the phase angle of 270° is expected and confirmed by the measurement in figure 5.

The divertor profiles show a moderate level of strike point splitting even before the application of external magnetic perturbation in some high δ discharges. The profiles show nearly monotonic decay, i.e., no strike point splitting, during the early stage of the discharge typically until $t \sim 200$ ms and then begin to develop local peaks and valleys in the scrape-off layer region. The degree of splitting varies in time, and both the heat flux and D_α profiles show similar evolution. We refer to this as “intrinsic strike point splitting”. As a possible source of the 3-D magnetic perturbation, the intrinsic error field from the non-circularity of poloidal field coils was considered. It was recently shown [20] that the PF5 coil in NSTX produces error fields with $n=3$ component as a dominant component. The inclusion of PF5 non-circularity in the vacuum field line tracing is therefore expected to produce a dominant $n=3$ field

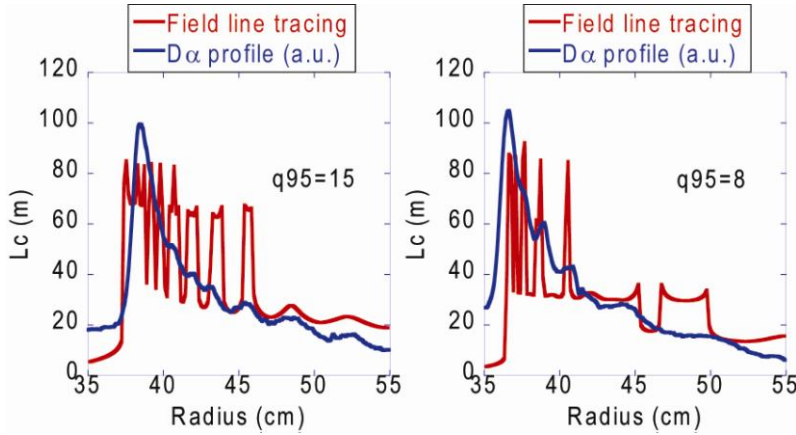


Figure 7 Comparison of connection length (red) with divertor D_α (blue) profiles in an $n=3$ application case. High q_{95} (left) and low q_{95} (right).

that intrinsic error fields may be one of the sources of the intrinsic strike point splitting. However, for some other discharges, intrinsic strike point splitting is not observed during the whole plasma duration time. It appears that the temporal evolution of the intrinsic strike point splitting agrees reasonably well with that of PF5 coil current, i.e., higher PF5 coil current is associated with higher degree of intrinsic strike point splitting. The correlation is an active area of research.

3.2 Effect of parameter changes on the divertor profile modification; q_{95} and n -number

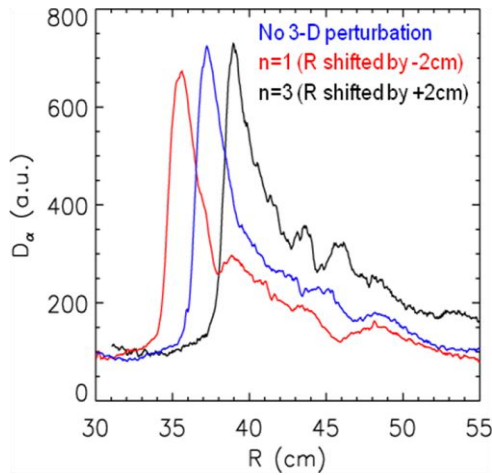


Figure 8 Measured D_α profiles at toroidal angle of 255° with no 3-D field (blue), $n=1$ field (red), and $n=3$ field (black) applied.

magnetic perturbation are also expected to produce different strike point splitting pattern in the divertor profiles. Field line tracing shows more split strike points with higher n -numbers. In figure 8, the D_α profile for $n=3$ perturbation has more pronounced local peaks than those for $n=1$ perturbation, while the unperturbed profile is relatively smoother than the other two.

structure although the model contains all non-circular components. Figure 6 shows a comparison of computed connection length profiles between the $n=3$ application and the PF5 intrinsic error field cases; the radial locations of the local peaks are in good agreement. This indicates

The poloidal spectrum produced by the midplane coils is roughly fixed with the given coil geometry. Thus a scan of safety factor, q_{95} , was carried out by changing plasma current, to see the effect on the divertor profile modification. Field line tracing indicates that plasmas with higher q_{95} produce more striations than those with lower q_{95} . This is experimentally confirmed, as shown in figure 7. The measured D_α profiles have more local peaks and valleys for $q_{95}=15$ than $q_{95}=8$; and they are in good agreement with connection length profiles from the vacuum field line tracing. Different toroidal mode (n) numbers of the applied

3.3 Heat flux deposition during ELMs triggered by application of 3-D fields

Externally imposed 3-D fields with sufficient amplitude trigger ELMs and strong heat and particle expulsion to the divertor plates. The frame speed of our IR camera was sufficient (1.6-3.8kHz) to resolve heat flux profiles during the ELM. The left plot of figure 9 shows the calculated heat flux profiles at the ELM peak and immediately (0.7ms) before the ELM occurrence in case of $n=3$ application. One can notice that the strike point splitting is persistent even during the ELM ($t=376.7\text{ms}$) as the profile exhibits local peaks and valleys. Also, the radial location of the split strike points before and during the ELM agrees. This indicates that the heat flux profile from ELMs triggered by $n=3$ fields follows the imposed field structure. The right plot of figure 9 shows the heat flux profiles across an ELM triggered by an $n=1$ field

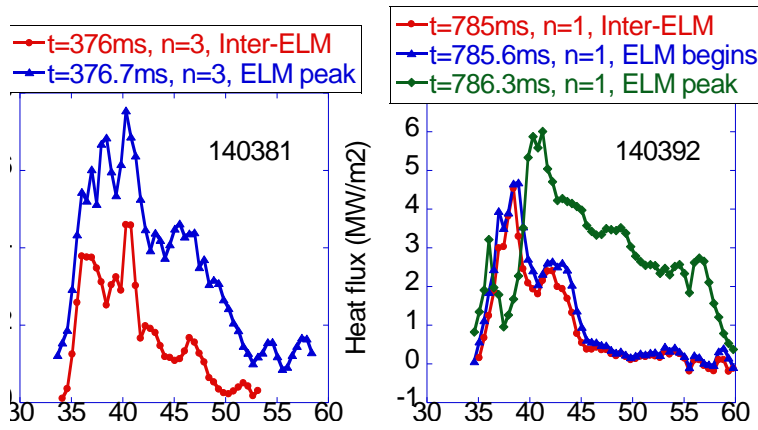


Figure 9 Measured heat flux profiles before and after an ELM occurrence with $n=3$ (left) and $n=1$ (right) fields applied.

application, showing a similar, but weaker phase locking than the $n=3$ case. We need to further examine higher n -numbers to confirm if the characteristics of the triggered ELMs are really determined by the imposed 3-D fields, not by the possibility of most unstable modes at low- n numbers for the ELM occurrence in NSTX.

4. Summary and conclusions

The non-axisymmetric perturbation fields are observed to break axisymmetry of the divertor heat and particle deposition and to cause the splitting of the strike point in NSTX. The applied 3-D fields modify heat and particle flux profiles in a manner consistent with vacuum field line tracing. Measurements taken for different phase angles of the applied $n=1$ perturbation fields provide the most direct evidence of the breaking of axisymmetry. The inclusion of plasma response inside the separatrix in the field line tracing does not significantly change the radial location and spacing of split strike points. This is important because it indicates that vacuum field line tracing may be sufficient to predict the structure of the generated strike point splitting under certain conditions. The intrinsic strike point splitting

observed in divertor profiles for some NSTX discharges is thought to be related to the intrinsic error fields in PF5 coil. The non-circularity of PF5 coil was modelled to be included in the vacuum field line tracing and was shown to generate similar field structure to the case of $n=3$ field application. The location of local peaks and valleys measured in the divertor profiles is consistent with the long parallel connection length in the field line tracing calculation. Heat flux profiles measured at the peak of triggered ELMs imply that the structure of split strike points may be persistent even during the ELMs and the heat flux follows imposed field structure, indicating that the ELMs may be phase-locked to the externally imposed perturbation.

Acknowledgements

This work was funded by the US Department of Energy, contract numbers DE-AC05-000R22725, DE-AC52-07NA27344(LLNL), and DE-AC02-09CH11466. We thank A. Herrmann and IPP-Garching for use of the THEODOR heat conduction code.

References

- [1] T. E. Evans, R. K. W. Roeder, J. A. Carter, B. I. Rapoport, M. E. Fenstermacher and C. J. Lasnier, *J. Phys : Conf. Ser.* **7** (2005) 174-90
- [2] O. Schmitz, T. E. Evans, M. E. Fenstermacher, *et al*, *Plasma Phys. Control. Fusion* **50** (2008), 124029
- [3] M. W. Jakubowski, T. E. Evans, M. E. Fenstermacher, *et al*, *Nucl. Fusion* **49** (2009) 095013
- [4] J-W. Ahn, J. M. Canik, R. Maingi, *et al*, *Nucl. Fusion* **50** (2010), 045010
- [5] T. E. Evans, R. A. Moyer, K. H. Burrell, *et al*, *Nature Phys.* **2** (2006) 419-23
- [6] Y. Liang, H. R. Koslowski, P. R. Thomas, *et al*, *Nucl. Fusion* **50** (2010), 025013
- [7] A. Kirk, E. Nardon, R. Akers, *et al*, *Nucl. Fusion* **50** (2010), 034008
- [8] J. M. Canik, R. Maingi, T. E. Evnas, *et al*, *Nucl. Fusion* **50** (2010) 034012
- [9] R. Maingi, T. H. Osborne, B. P. LeBlanc, *et al*, *Phys. Rev. Lett.* **103** (2009) 075001
- [10] J. M. Canik, R. Maingi, T. E. Evnas, *et al*, *Phys. Rev. Letts.* **104** (2010) 045001
- [11] S. A. Sabbagh, R. E. Bell, J. E. Menard, *et al*, *Phys. Rev. Lett.* **97** (2006) 045004
- [12] J. E. Menard, M. G. Bell, R. E. Bell, *et el*, *Nucl. Fusion* **47** (2007) S645
- [13] J-W. Ahn, R. Maingi, D. Mastrovito, and A. L. Roquemore, *Rev. Sci. Instrum.* **81** (2010) 023501
- [14] A. G. McLean, *et al*, *Rev. Sci. Instrum.*, In press (2010)
- [15] A. Herrmann, W. Junker, K. Gunther, *et al*, *Plasma Phys. Control. Fusion* **37** (1995) 17
- [16] V. A. Soukhanovskii, A. L. Roquemore, C. H. Skinner, *et al*, *Rev. Sci. Instrum.* **74** (2003) 2094
- [17] V. A. Soukhanovskii, R. E. Bell, C. Bush, *et al*, *J. Nucl. Maters* **390-391** (2009) 516-519
- [18] J. M. Canik, *et al*, Proceedings of the 13th International Conference on Plasma Surface Interaction, May 2010, San Diego, USA
- [19] J.-K. Park, , A. H. Boozer, and A. H. Glasser, *et al*, *Phys. Plasmas* **14** (2007) 052110
- [20] J. E. Menard, R. E. Bell, D. A. Gates, *et al*, *Nucl. Fusion* **50** (2010) 045008